# Dalton Transactions

Accepted Manuscript






ROYAL SOCIETY OF CHEMISTRY

www.rsc.org/dalton

# Table of Contents

## Advanced $Cd^{II}$ Complexes as High Efficiency Co-Sensitizers for Enhanced Dye-Sensitized Solar Cells Performance

**Song Gao,[a] Rui Qing Fan,*[,a] Xin Ming Wang,[a] Liang Sheng Qiang,[a] Li Guo Wei,[a] Ping Wang,[a] Yu Lin Yang,*[,a] Yu Lei Wang[b]**

[a] *Department of Chemistry, Harbin Institute of Technology, Harbin 150001, P. R. China*

[b] *National Key Laboratory of Science and Technology on Tunable Laser, Harbin Institute of Technology, Harbin 150080, P. R. China*

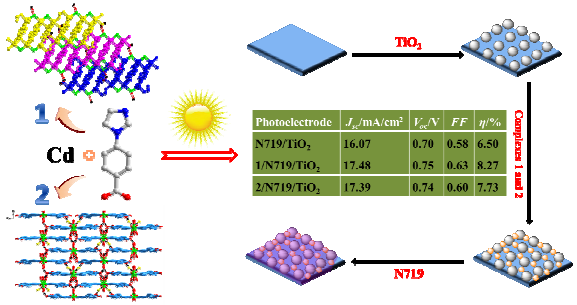


| Photoelectrode | $J_{sc}$/mA/cm² | $V_{oc}$/V | *FF* | $\eta$/% |
|---|---|---|---|---|
| N719/$TiO_2$ | 16.07 | 0.70 | 0.58 | 6.50 |
| 1/N719/$TiO_2$ | 17.48 | 0.75 | 0.63 | 8.27 |
| 2/N719/$TiO_2$ | 17.39 | 0.74 | 0.60 | 7.73 |

The prepared complexes **1** and **2** can serve as co-sensitizers to enhance the power-conversion efficiency.

# Advanced $Cd^{II}$ Complexes as High Efficiency Co-Sensitizers for Enhanced Dye-Sensitized Solar Cells Performance

**Song Gao,[a] Rui Qing Fan,*[,a] Xin Ming Wang,[a] Liang Sheng Qiang,[a] Li Guo Wei,[a] Ping Wang,[a] Yu Lin Yang,*[,a] Yu Lei Wang[b]**

[a] *Department of Chemistry, Harbin Institute of Technology, Harbin 150001, P. R. China*

[b] *National Key Laboratory of Science and Technology on Tunable Laser, Harbin Institute of Technology, Harbin 150080, P. R. China*

**To whom the proofs and correspondence should be sent.**

Professor Rui-Qing Fan
Department of Chemistry
Harbin Institute of Technology Harbin 150001, P. R. China
Fax: +86-451-86413710
E-mail: fanruiqing@hit.edu.cn and ylyang@hit.edu.cn

† Electronic supplementary information (ESI) available: Experimental details and results of PXRD, TGA, TA and IR experiments. The CIF files give crystallographic data for complexes **1** and **2**. Fig. S1–S4 and Tables S1–S3. CCDC 1041927 and 1041928. For ESI and crystallographic data in CIF or other electronic format see DOI: 10.1039/000000x

## Abstract

This work reports on two new complexes with generally formula of $[Cd_3(IBA)_3(Cl)_2(HCOO)(H_2O)]_n$ **(1)** and $\{[Cd_{1.5}(IBA)_3(H_2O)_6]\cdot 3.5H_2O\}_n$ **(2)**, which can be synthesized with reactions of $Cd^{II}$ with a rigid linear ligand 4-HIBA containing imidazolyl and carboxylate functional groups [4-HIBA = 4-(1H-imidazol-1-yl)benzoic acid]. Single-crystal X-ray diffraction analyses indicates that complex **1** is a 2D "wave-like" layer structure constructed from trinuclear units and complex **2** is just a mononuclear structure. Surprisingly, both complexes **1** and **2** appear as 3D supramolecular network via intermolecular hydrogen bonding interactions. What's more, due to their strong UV-visible absorption, **1** and **2** can be employed as co-sensitizers in combination with N719 to enhance the dye-sensitized solar cells (DSSCs) performance. Both of them could overcome the deficiency of ruthenium complex N719 absorption in the region of ultraviolet and blue-violet, and the charge collection efficiency is also improved when **1** and **2** are used as co-sensitizers, which are all in favor of enhancing the performance. The DSSC devices using co-sensitizers of **1**/N719 and **2**/N719 show the overall conversion efficiency of 8.27% and 7.73% with short circuit current density of 17.48 mA $cm^{-2}$ and 17.39 mA $cm^{-2}$, open circuit voltage of 0.75 V and 0.74 V, respectively. The overall conversion efficiency is 27.23% and 18.92% higher than that of a device solely sensitized by N719 (6.50%). Consequently, the prepared complexes are high efficiency co-sensitizers for enhancing the performance of N719 sensitized solar cells.

## Introduction

There is an ever growing interest in developing metal coordination complexes (MCCs) for application in photovoltaic performance.[1] The main difficulty in improving the efficiency of photovoltaic energy conversion lies in the spectral mismatch between the energy distribution of photons in the incident solar spectrum and the band-gap of a semiconductor material.[2] Co-sensitization is an effective approach to enhance the device performance through a combination of two or more dyes sensitized the same semiconductor film together, extending the light harvesting spectrum.[3] Ruthenium complex N719 as a typical representative of organic dye used in DSSC has low utilization in the region of short wavelength. Enhancing N719 absorption efficiency of the full-spectrum sunlight still remains a great challenge in this field.[4] For this reason, MCCs with strong absorption in the short wavelength region are being applied in the DSSC as co-sensitizers. The key to design photoelectric MCCs is the matching of organic ligand and central metal ion in order to provide the platform to generate ultraviolet absorption.[5-8]

Organic ligands with N and/or O donors often have been employed as effective building blocks in the construction of metal coordination complexes.[9,10] Among the organic ligands, the rigid ligand 4-(1H-imidazol-1-yl)benzoic acid with π-conjugated system play crucial roles in determining the structure and ultraviolet absorption of the MCCs because of the diversiform coordination mode and the flexible nature of N and/or O donors.[11-15] The enormous variability of available ligand–metal combinations opens the possibility of creating photovoltaic materials "by design". $Cd^{II}$ has been chosen as an excellent participant for construction of complexes because of its relatively low-cost (compared to $Ir^{III}$, $Ru^{II}$, $Os^{II}$ and $Pt^{II}$, which are used as common co-sensitizers).[16-20] On the basis of the above considerations, our group designed low-cost $Cd^{II}$ complexes to replace precious metal coordination complexes as co-sensitizers.[21]

In this report, we have successfully designed and synthesized two new $Cd^{II}$ complexes, $[Cd_3(IBA)_3(Cl)_2(HCOO)(H_2O)]_n$ **(1)**, $\{[Cd_{1.5}(IBA)_3(H_2O)_6]\cdot 3.5H_2O\}_n$ **(2)**. Since the strong absorption in 300-400 nm, **1** and **2** were selected to be a co-sensitizer and applied in the DSSC system sensitized by N719, respectively. It showed that the absorption spectra of **1** and **2** could compensate for that of N719 in region of

ultraviolet and blue-violet, and thus, the light harvesting was enhanced. This results in 27.23% and 18.92% improvement of DSSCs performance. Therefore, **1** and **2** are promising candidates as co-sensitizers for high efficiency DSSCs. This strategy may provide interesting insight into the development of high-performance DSSCs devices.

## Results and discussion

### Structure description: $[Cd_3(IBA)_3(Cl)_2(HCOO)(H_2O)]_n$ (1)

Structural analysis indicates that **1** is a trinuclear 2D "wave-like" layer structure. The relevant asymmetric unit consists of three crystallographically independent $Cd^{II}$ cations, three $IBA^-$ anions, two chloride anions, one $HCOO^-$ anion and one coordinated water molecule (Fig. 1a). The central Cd2 cation is linked to two unsymmetry-related terminal Cd1 and Cd3 cations by two chloride ions to afford a linear trinuclear unit with Cd1···Cd2 distance of 3.622(1) Å and Cd2···Cd3 distance of 3.985(1) Å. The Cd1 and Cd2 are located in distorted $\{CdNO_4Cl\}$ and $\{CdNO_3Cl_2\}$ octahedral geometry, respectively. The Cd3 is coordinated with three oxygen atoms and one nitrogen atom from $IBA^-$ and $HCOO^-$ anions, forming slightly distorted trigonal bipyramid geometry along with one chloride anion (Fig. 1b). In the trinuclear cluster, the distances of Cd−O [2.236(4) Å−2.488(4) Å], Cd−N [2.234(4) Å−2.272(4) Å] and Cd−Cl [2.522(2) Å−2.692 (2) Å] are in the normal ranges of those reported $Cd^{II}$ complexes previously,[22,23] and bond angles around the central Cd(II) ion vary from 50.5(1)°−173.5(1)°. The neighbouring trinuclear units ($Cd1_{oct}$–$Cd2_{oct}$–$Cd3_{penta}$) are connected with one $HCOO^-$ anion, forming a 1D straight chain (Fig. 1c). Each $IBA^-$ anion links two adjacent cadmium cations to form another 1D "wave-like" chain structure (Fig. 1d). The carboxylate group of the different $IBA^-$ anions adopts chelate coordinated mode and chelate-monatomic bridge coordinated mode, respectively. Two adjacent chains are interconnected to construct a 2D "wave-like" layer structure (Fig. 1e).

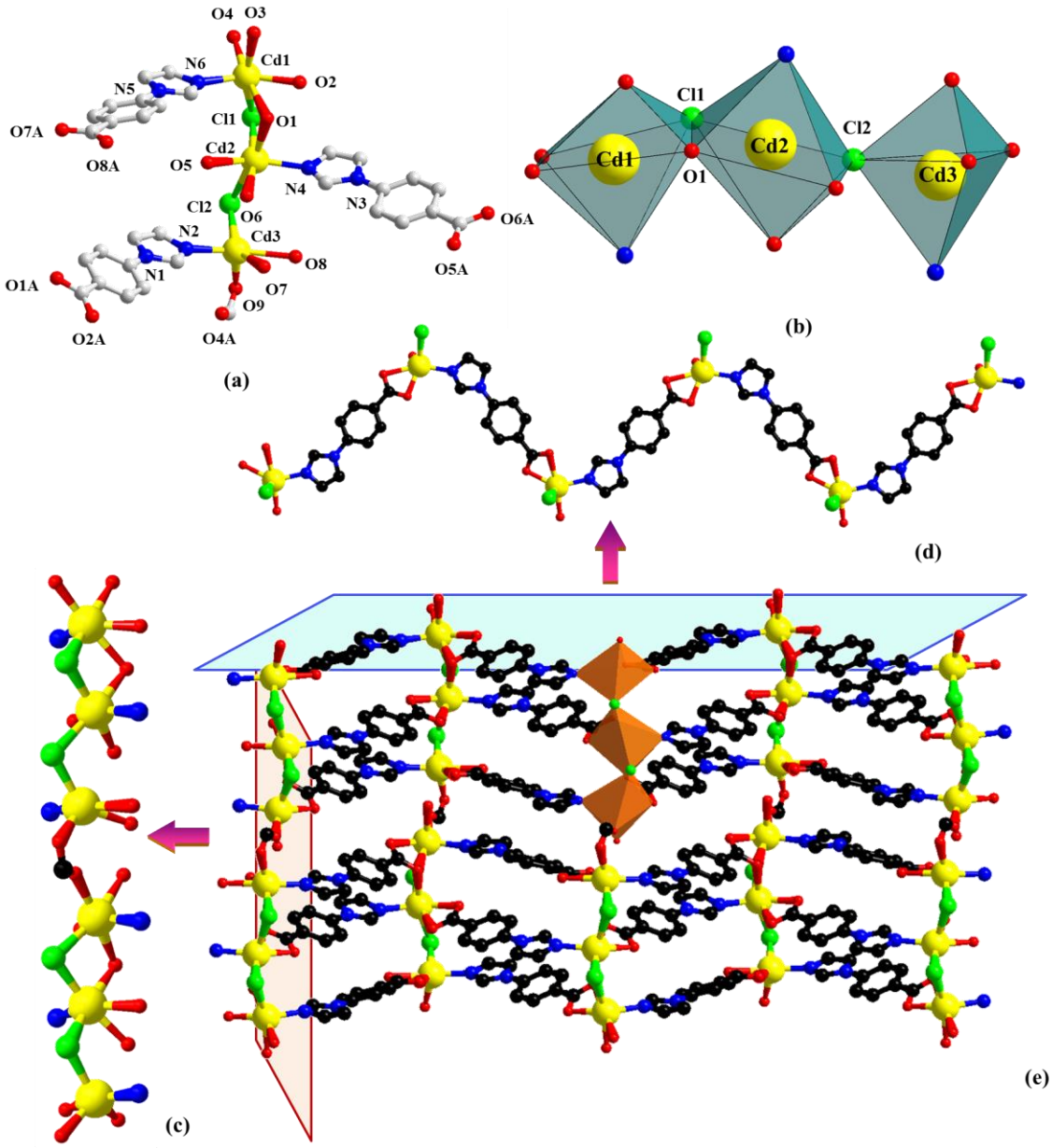


**Fig. 1** (a) The molecular structure of complex **1**. All hydrogen atoms have been omitted for clarity. (b) Polyhedral representation of the coordination sphere of the $Cd^{II}$ centre in **1**. (c) The 1D straight chain composed of the trinuclear units in **1**. (d) Ball–and–stick representation of the 1D "wave-like" chain in **1**. (e) Polyhedral and ball–and–stick representation of the 2D layer in **1**.

If coordinated water molecule was ignored, and the $Cd^{II}$ cation considered as the node, three $IBA^{-}$ anions, two chloride anions and one $HCOO^{-}$ anion as the linkers, the simplified topological representation of the **1** exhibits a 4-connected 2D "wave-like" sql topological type, which is described in Fig. 2a. It is noteworthy that the 2D sheets are arranged in an interesting 3D supramolecular network via O3-H3A···O7 and O3-H3C···Cl2 intermolecular hydrogen bonding interactions (Fig. 2b).

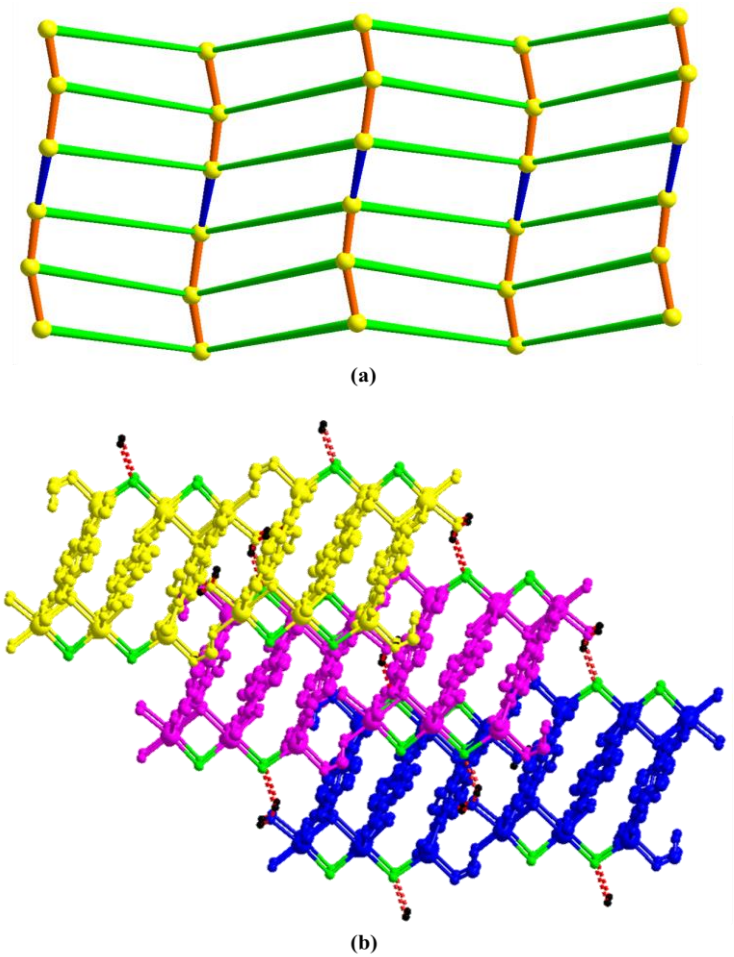


**Fig. 2** (a) The 2D sql topology in its most symmetrical form distinguished by different colors ($Cd^{II}$, yellow ball; $IBA^{-}$, green linker; $Cl^{-}$, organic linker; $HCOO^{-}$, blue linker) (b) A 3D supramolecular structure of **1** (hydrogen bonding is red dashed line).

## Structure description: $\{[Cd_{1.5}(IBA)_3(H_2O)_6]\cdot 3.5H_2O\}_n$ (2)

The result of X-ray diffraction analysis revealed that complex **2** consists of one and a half $Cd^{2+}$ cations, three $IBA^{-}$ anions, six coordination water molecules and three and a half free water molecules, which is shown in Fig. 3a. Each $Cd^{II}$ cation is six-coordinated by four oxygen atoms and two nitrogen atoms from four coordination water molecules and two $IBA^{-}$ anions, resulting in slightly distorted octahedron geometry (Fig. 3b). Cd–O bond lengths range from 2.265(3) Å to 2.388(2) Å and Cd–N bond lengths vary from 2.269(2) Å to 2.293(2) Å, respectively. O–Cd–O bond angles range from 81.2(6)° to 180.0(1)° and O–Cd–N bond angles are in the range of 84.1 (7)°–99.7 (7)°, respectively. Each $Cd^{II}$ cation links two $IBA^{-}$ anions and four coordinated water molecules to form a mononuclear structure. In complex **2**, the distance of O–H···O is in the range from 1.860 to 2.034 Å. A 3D supramolecular network is formed by O–H···O hydrogen bonded interactions (Fig. 3c).

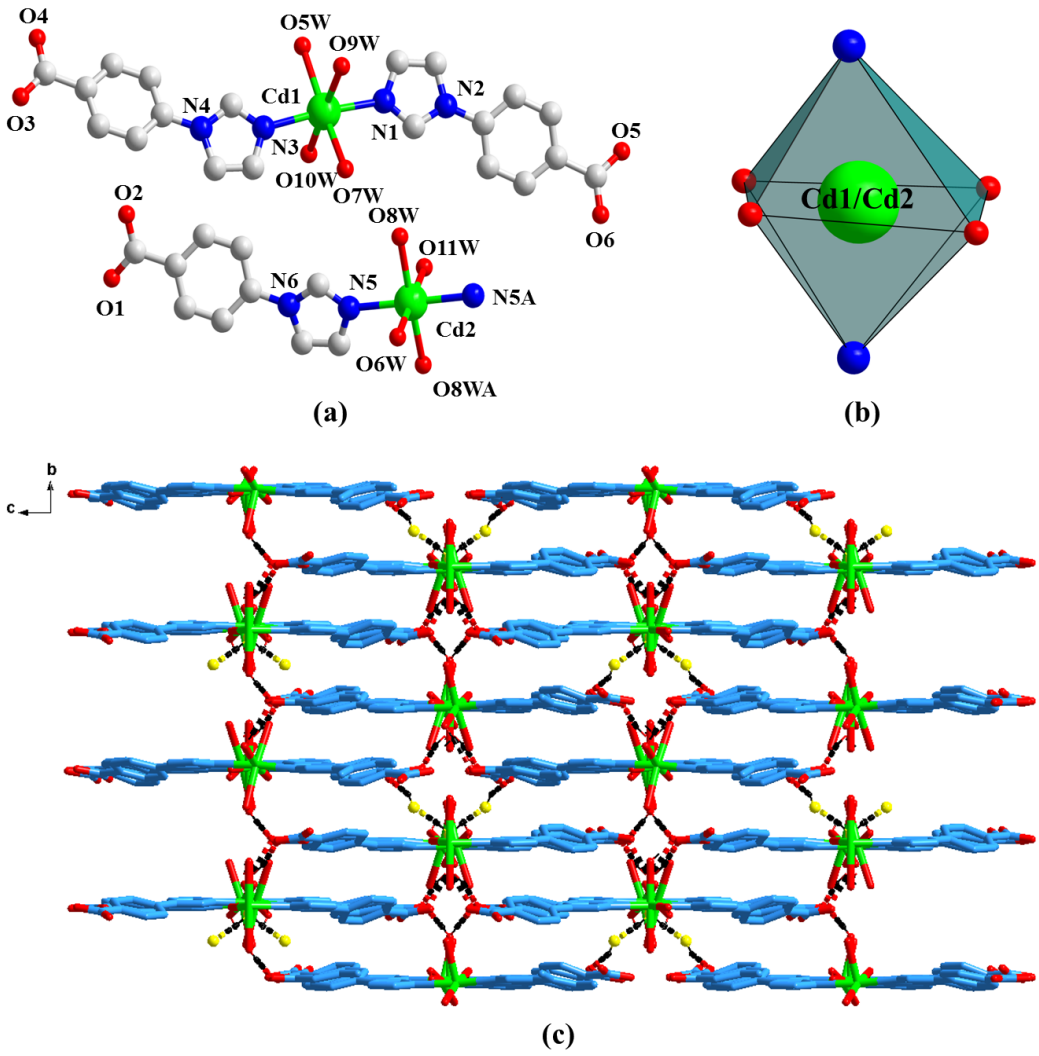


**Fig. 3** (a) The molecular structure of complex **2**. All hydrogen atoms and free water molecules have been omitted for clarity. (b) Polyhedral representation of the coordination sphere of the $Cd^{II}$ centre in **2**. (c) A 3D supramolecular structure of **2** (hydrogen bonding is black dashed line).

## Powder X-ray diffraction (PXRD) and thermal analysis of complexes 1 and 2

PXRD has been used to check the phase purity of the bulky samples in the solid state. As shown in Fig. S1, the experimental PXRD patterns of complexes **1** and **2** are in good agreement with the simulated patterns, which indicate the good phase purity of complexes **1** and **2**.[24] The differences in intensity may be due to the preferred orientation of the crystalline powder samples. Thermogravimetric experiments were conducted to study the thermal stability of complexes **1** and **2** (Fig. S2).[25] For **1**, the first weight loss of 12.05% from 63 °C to 151 °C is attributed to the release of one coordinated water molecule, two HCl molecules and one HCOOH molecule (calcd: 13.26%).[26] The second weight loss of 53.14% (calcd: 54.67%) from 153 °C corresponds to the loss of three 4-HIBA ligands. **2** displays two weight loss steps. The

first of 17.64% from 126 °C to 257 °C, is assigned to the loss of six coordination water molecules and three and a half free water molecules (calcd: 18.99%). The second weight loss of 61.21% from 266 °C to 402 °C corresponds to the decomposition three 4-HIBA ligands (calcd: 62.64%).

**Optical properties of complexes 1 and 2**

The absorption spectra of **1** and **2** in ethanol are shown in Fig. 4 and their absorption data are listed in Table 1. The two prepared complexes display strong absorption peaks at ca. 334 nm with weak shoulder absorption bands at around 372 nm. In comparison to the absorption of N719 in ethanol (Fig. 4), the absorption spectra of **1** and **2** could compensate for that of N719 in the wavelength region of ultraviolet and blue-violet. Encouraged by above test, **1** and **2** can be considered as co-sensitizers used in N719 sensitized DSSCs. The molar extinction coefficients in the blue-violet region are 48,709 $M^{-1}$ $cm^{-1}$ for **1** and 44,770 $M^{-1}$ $cm^{-1}$ for **2**. All of these are much higher than that of the ruthenium complex N719.[27,28] A higher molar extinction coefficient indicates that the **1** and **2** possess higher light harvesting ability in this wavelength region compared with N719 and $I_3^-$ (25,000$M^{-1}$ $cm^{-1}$).[29] Hence it can be predicted that the photon lost due to the light absorption by $I_3^-$ will be suppressed by the use of **1** or **2** as a co-sensitizer.

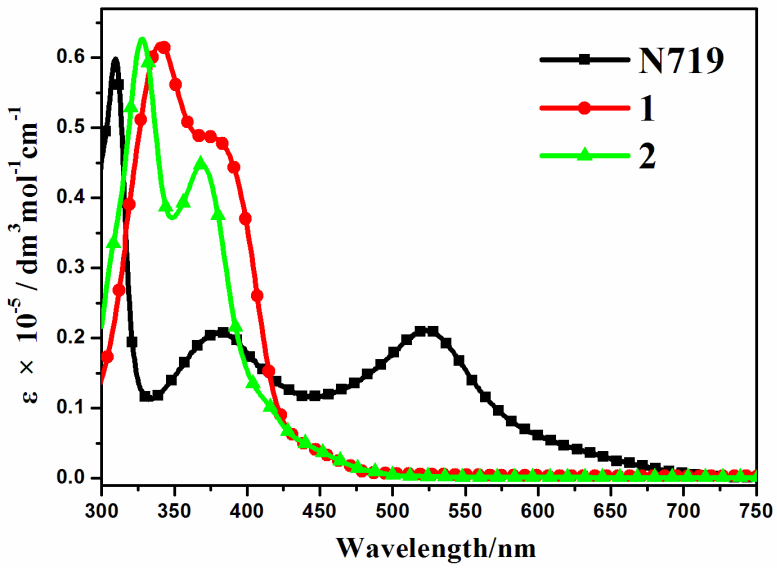


**Fig. 4** UV-visible absorption spectra of **1**, **2** and N719 in ethanol.

To further investigate whether the prepared complexes are suitable for use in DSSCs, the absorption spectra of **1**/N719 and **2**/N719 co-sensitized $TiO_2$ films are recorded and shown in Fig. 5. The absorption of N719 on $TiO_2$ film in visible light

region is remarkably broadened due to the electronic coupling of the dyes on the $TiO_2$ surface.[30] When N719 was combined with **1** or **2**, respectively, its absorption in the region of 350-500 nm on $TiO_2$ film was enhanced. The enhancement of absorption in the region of 350-500 nm is consistent with the result that the prepared complexes could compensate for that of N719 in the wavelength region of the visible spectrum in solid state.

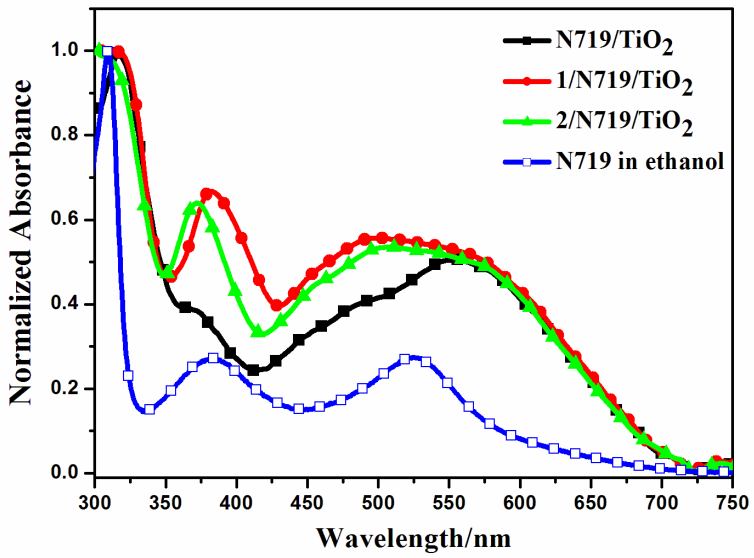


**Fig. 5** UV-visible absorption spectra of **1**, **2** and N719 on $TiO_2$ films.

## Electrochemical properties of complexes 1 and 2

Energy matching is crucial in selecting sensitizers for DSSCs. Therefore, cyclic voltammetry (CV) experiments were carried out to determine the highest occupied molecular orbital (HOMO) levels and the lowest unoccupied molecular orbital (LUMO) levels of the two prepared complexes and the experimental data are also summarized in Table 1. The HOMO values for **1** and **2** are evaluated to be -5.31 and -5.39 eV, respectively. As calculated from the edge of absorption spectra, the excitation transition energies ($E_{0-0}$) for **1** and **2** are 3.12 and 3.18 eV, respectively. Therefore, the LUMO levels of **1** and **2** are calculated to be -2.19 and -2.21 eV, respectively.[31] The LUMO level of a sensitizer should lie above the conduction band (CB) of the $TiO_2$ semiconductor (-4.40 eV vs. vacuum) for efficient electron injection, and its HOMO energy level should lie below the energy level of the $I^-/I_3^-$ redox couple (-4.85 eV vs. vacuum) for regeneration. The LUMO levels of the complexes **1** and **2** are higher than that of N719 and the conduction band of $TiO_2$, which result in an enhanced injection driving force of electrons compared with sole N719. Thus, the positive synergistic effect of these complexes and N719 improves the electrons

injection efficiency from the LUMO of dye to the conduction band of $TiO_2$. The HOMO and LUMO energy levels of **1** and **2** are shown in Scheme 1. It shows that the energy levels of **1** and **2** are appropriate for the DSSCs system containing $TiO_2$.[32]

**Table 1** Experimental data for spectral and electrochemical properties of the complexes **1** and **2**

| Dyes | $\lambda_{abs}$(nm)[a] | $\varepsilon(M^{-1}cm^{-1})$[a] | $\lambda_{em}$(nm)[a,b] | $E_{0-0}$(eV)[c] | $E_{ox}$/V vs SCE[d] | $E_{HOMO}$(eV)[e] | $E_{LUMO}$(eV)[e] |
|---|---|---|---|---|---|---|---|
| **1** | 375 | 48709 | 436 | 3.12 | 0.91 | –5.31 | –2.19 |
| **2** | 369 | 44770 | 408 | 3.18 | 0.99 | –5.39 | –2.21 |

[a] Absorption and emission spectra were recorded in ethanol solution ($10^{-5}$ M) at room temperature.
[b] Complexes were excited at their absorption maximum value
[c] Optical band gap calculated from intersection between the absorption and emission spectra.
[d] The first oxidation potentials of complexes were obtained by CV measurement.
[e] The values of $E_{HOMO}$ and $E_{LUMO}$ were calculated with the following formula:[33]
HOMO (eV) = -e($E^{ox}_{onset}$ V + 4.4V); LUMO (eV) = $E_{HOMO}$ + $E_{0-0}$
where $E_{0-0}$ is the intersection of absorption and emission of the complexes **1** and **2**.

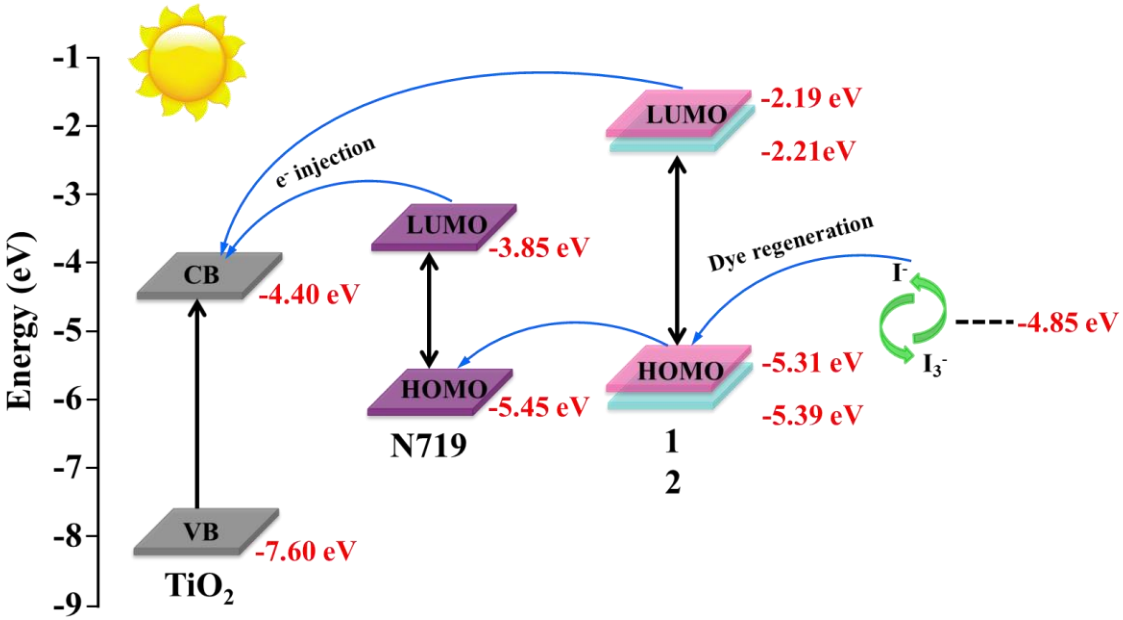


**Scheme 1.** Schematic energy diagram of HOMO and LUMO for dyes compared to the energy levels calculated for $TiO_2$.

## Photovoltaic properties of DSSCs

The two prepared complexes were employed as co-sensitizers to assemble co-sensitized DSSCs, which were fabricated following a stepwise co-sensitization procedure by sequentially immersing the $TiO_2$ electrode (with a thickness of ca. 10 μm) in a separate solution of N719 and prepared complexes. For comparison purpose, devices sensitized by individual dye N719 were also fabricated under the same experimental conditions. The photocurrent-voltage (*J-V*) characteristics of the devices co-sensitized by **1**/N719 and **2**/N719 as well as solely sensitized by N719 under

illumination (AM 1.5G, 100 mW $cm^{-2}$) are shown in Fig. 6, and the corresponding cell performances are summarized in Table 2. The individually N719 sensitized device is found to exhibit an overall conversion efficiency ($\eta$) value of 6.50% (with $J_{sc}$ = 16.07 mA $cm^{-2}$, $V_{oc}$ = 0.70 V, and $FF$ = 0.58). This low performance compared to the previous reports could be due a single thin transparent $TiO_2$ film used in these devices. The individually complexes **1** and **2** sensitized device exhibited $\eta$ value of 2.19% (with $J_{sc}$ = 6.36 mA $cm^{-2}$, $V_{oc}$ = 0.59 V, and $FF$ = 0.58) and 2.02% (with $J_{sc}$ = 6.04 mA $cm^{-2}$, $V_{oc}$ = 0.59 V, and $FF$ = 0.56), respectively. The lower $\eta$ value for devices sensitized by the complexes co-sensitizers individually is obviously attributed to their narrow adsorption band. However, the co-sensitized solar cell devices **1**/N719 and **2**/N719 showed an efficiency of 8.27% (with $J_{sc}$ = 17.48 mA $cm^{-2}$, $V_{oc}$ = 0.75 V, and $FF$ = 0.63) and 7.73% (with $J_{sc}$ = 17.39 mA $cm^{-2}$, $V_{oc}$ = 0.74 V, and $FF$ = 0.60), respectively. The efficiency of the devices co-sensitized by **1**/N719 and **2**/N719 is 27.23% and 18.92% higher than that of cells sensitized by N719.

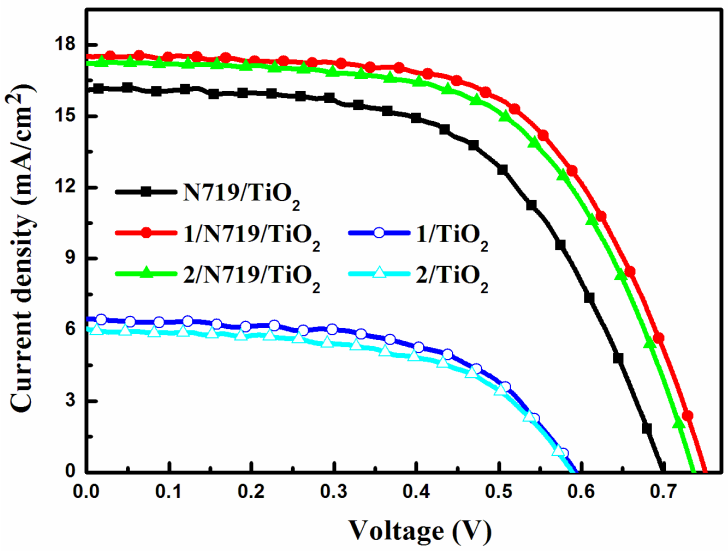


**Fig. 6** *J–V* curves for DSSCs based on co–sensitized photoelectrodes and N719, **1**, **2** sensitized photoelectrode under irradiation.

**Table 2** *J-V* performance of DSSCs based on different photoelectrodes

| Photoelectrode | $J_{sc}$/mA/$cm^2$ | $V_{oc}$/V | *FF* | $\eta$/% |
|---|---|---|---|---|
| N719/$TiO_2$ | 16.07 | 0.70 | 0.58 | 6.50 |
| **1**/$TiO_2$ | 6.36 | 0.59 | 0.58 | 2.19 |
| **2**/$TiO_2$ | 6.04 | 0.59 | 0.56 | 2.02 |
| **1**/N719/$TiO_2$ | 17.48 | 0.75 | 0.63 | 8.27 |
| **2**/N719/$TiO_2$ | 17.39 | 0.74 | 0.60 | 7.73 |

Dark-current measurement of DSSCs has been considered as a qualitative technique to describe the extent of the back electron transfer. A comparison of dark current between the investigated cells can provide useful information regarding the back electron transfer process. Fig. 7 shows the dark current–voltage characteristics of the DSSCs based on different photoelectrodes. The onset potential of the dark current for individual N719-sensitized DSSC occurs at a bias about +0.44 V, with a subsequent dramatic increase of dark current with the increase of potential. In contrast, for the co-sensitized DSSCs, the onset potential shifted to about +0.50 V for **1**/N719 and **2**/N719. The increase of the onset potential indicates that the complexes **1** and **2** could successfully suppress the electron back reaction with $I_3^-$ in the electrolyte.

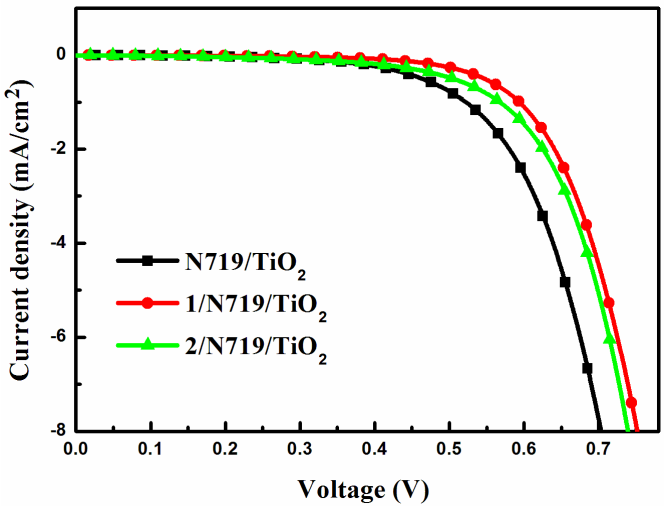


**Fig. 7** *J–V* curves for DSSCs based on co–sensitized photoelectrodes and N719 sensitized photoelectrode in dark.

The higher $\eta$ values of **1**/N719 and **2**/N719 co-sensitized solar cells are attributed to the enhanced photovoltaic parameters of $J_{sc}$ and $V_{oc}$. Generally, the $J_{sc}$ value is influenced by the incident photon-to-current conversion efficiency (IPCE) response of cells, since they are related by the equation:

$$J_{sc} = \int e\phi_{\text{ph.AM1.5G}}(\lambda)d\lambda$$

where $e$ is the elementary charge and $\phi_{\text{ph.AM1.5G}}$ is the photon flux at AM 1.5 G, 100 mW/cm$^2$ irradiation.[34-36] The IPCE spectra of different devices are collected in Fig. 8. The DSSCs containing only N719 dye have a broad IPCE spectrum from 300-750 nm but a decrease in the wavelength range of 340-420 nm, which is due to the competitive light absorption between $I_3^-$ and N719. When the prepared complexes are used as co-sensitizer, the IPCE spectrum in the whole visible region is enhanced. This can be attributed to the fact that the prepared complexes have attached to the $TiO_2$

surface effectively and contributed to the electron injection into the conduction band of the $TiO_2$. This means the co-sensitization of N719 and new complexes have significant synergy and compensatory effects on the light harvesting and electron injection. Based on the IPCE and the absorption spectra, the cells' higher $J_{sc}$ in the case of co-sensitization are mainly ascribed to better light harvesting in the short wavelength region, where the absorption of N719 is compensated and the competitive light absorption of $I_3^-$ is overcome.

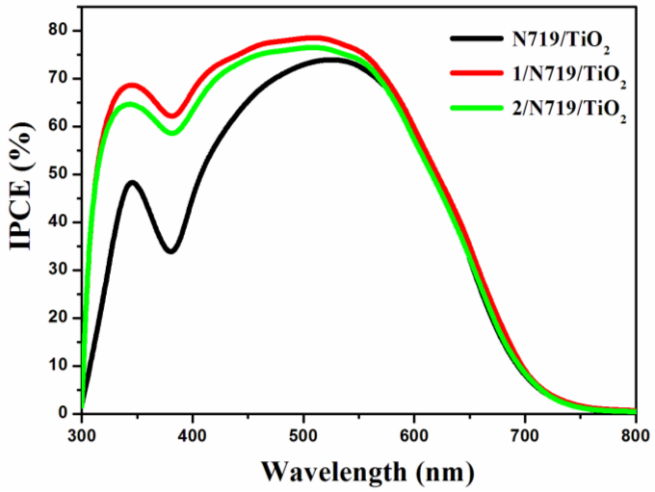


**Fig. 8** The incident photon-to-current conversion efficiency spectra of devices based on single N719 sensitized and co-sensitized photoanodes.

In order to investigate the charge injection dynamics in different DSSCs and further understand the underlying causes which result in different short circuit current density ($J_{sc}$), transient absorption (TA) spectroscopy was employed to characterize co-sensitized and single N719 sensitized solar cells. Also, additives co-sensitizers are known to affect the electron injection dynamics. The TA spectra of N719, **1**/N719 and **2**/N719 with the addition of an iodide-based electrolyte at 500 ps are shown in Fig. S3. The spectra show negative ground state bleaching features, which result from a decrease in absorption in the excited dye, less than 610 nm. The spectra are dominated by a broad photo-induced absorption (PA) band, which results from increased absorption of the excited dye, greater than 610 nm. This broad PA band is the convolution of two PA spectral features. We attribute one PA feature to the absorption of the excited-state dye (dye*) at approximately 650 nm, and the other to the absorption of the oxidized-dye ($dye^+$) at approximately 760 nm. The oxidized-dye is formed after charge injection occurs, and is therefore a probe of the ultrafast charge injection dynamics in DSSCs.[37,38] It is worth noting that after co-sensitization, at 760 nm ($dye^+$) there is an increase in the PA signal while at 650 nm (dye*) the PA signal

is unchanged, which indicates that the charge injection was enhanced after co-sensitization and resulted in enhanced $J_{sc}$. The increase in the PA signal at 760 nm further confirmed that the electron injection from the photo-excited states of dye to the conduction band of $TiO_2$ is thermodynamically favorable.

Under light illumination, electrochemical impedance spectroscopy (EIS) was utilized to analyze the charge transport resistance at the $TiO_2$/dye/electrolyte interface of DSSCs.[39,40] As shown in Fig. 9a, the two semicircles located in high and middle frequency regions (left to right) are attributed to the electrochemical reaction at the Pt/electrolyte interface and the charge transfer at the $TiO_2$/dye/electrolyte interface. The radius of the large semicircle located in middle frequency regions in the Nyquist plots is decreased after co-sensitized with complex, and the values are in the order of **1**/N719 < **2**/N719 < N719. The electron transport time ($\tau_d$) is a measure of the average time taken by the injected electron to reach the collecting FTO electrode; a faster electron transport time is associated with a higher photocurrent.[41] It could also be calculated from the Bode phase plots of the EIS spectra of different solar cells (Fig. 9b), according to the relationship: $\tau_d = 1/(2\pi f_{max})$, where $f_{max}$ is the frequency at the maximum of the curve in the intermediate frequency region in Bode phase plot. The calculated values of the electron transport time ($\tau_d$) for different devices are 5.35 ms for **1**/N719, 6.22 ms for **2**/N719 and 8.68 ms for individually N719, respectively.

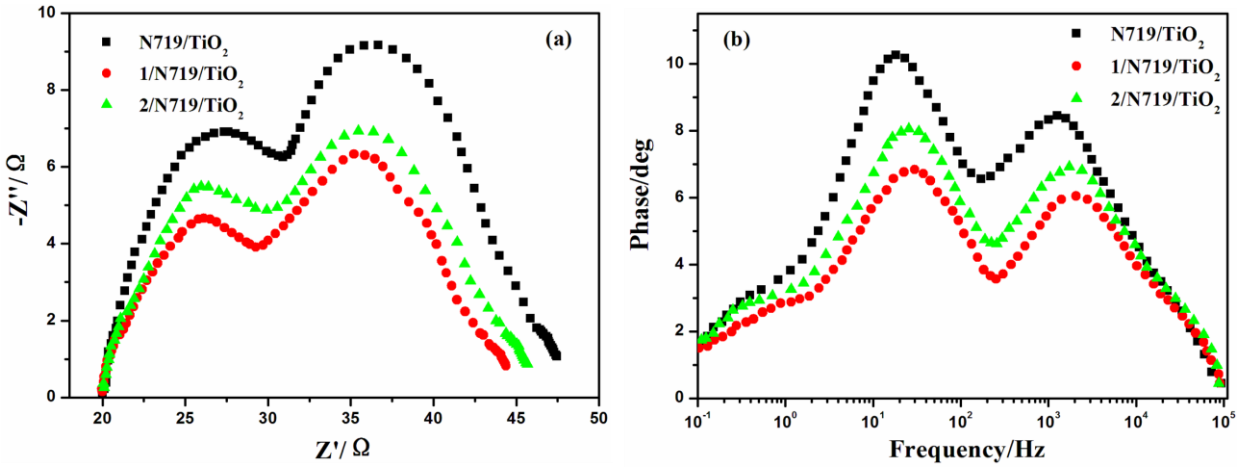


**Fig. 9** (a) Nyquist plots (b) Bode plots of EIS for DSSCs based on different photoelectrodes measured under standard AM1.5 G solar irradiation.

In dark conditions, as shown in Fig. 10a, the two semicircles located in high, middle and low frequency regions (left to right) of Nyquist plots are attributed to the redox reaction at the Pt counter electrode and the electron transfer at the $TiO_2$/dye/electrolyte interface. Therefore the larger semicircle observed in middle

frequency region represents the resistances of the charge transfer from the $TiO_2$ to the electrolyte. The radius of the semicircle observed in middle frequency range lies in the order of **1**/N719 > **2**/N719 > N719, which indicates an increase of electron recombination impedence and a reduction of the interfacial charge recombination rate.

In an effort to understand the enhancement of the $V_{oc}$ value in the dye-sensitized solar cells, the electron lifetimes ($\tau_e$) in different devices were calculated by fitting the Bode plots of the EIS spectra of different solar cells in dark (Fig. 10b), according to the relationship: $\tau_e = 1/(2\pi f_{max})$, where $f_{max}$ is the frequency at the maximum of the curve in the intermediate frequency region in Bode phase plot.[42] The electron lifetimes ($\tau_e$) for the devices co-sensitized with prepared complexes (19.49 ms for **1**/N719 and 17.53 ms for **2**/N719) were found to be longer than individually N719 sensitized device (13.40 ms). This difference might be expected, since the adsorption of prepared complexes may form a better dye coverage to passivate the $TiO_2$ surface or form an insulating molecular layer composed of prepared complexes and N719 molecules. It will reduce the recombination due to electron back-transfer. This retardation of the charge recombination between injected electron and $I_3^-$ ions in the electrolyte leads to a consequent increase of $V_{oc}$. This appears to be consistent with the larger $V_{oc}$ values sequence which is in the order of **1**/N719 > **2**/N719 > N719.

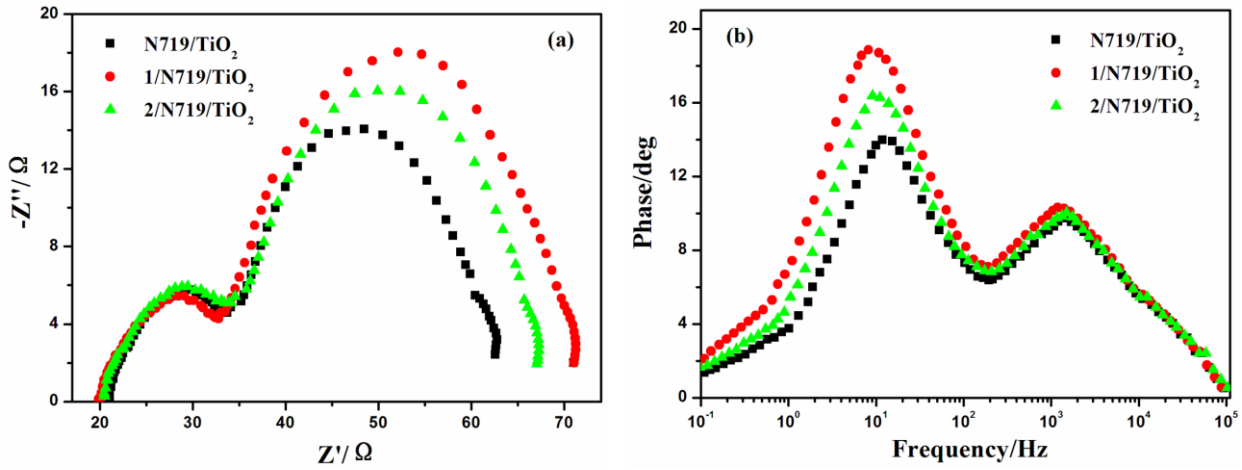


**Fig. 10** (a) Nyquist plots (b) Bode plots of EIS for DSSCs based on different photoelectrodes measured in dark conditions.

The charge collection efficiency ($\eta_{cc}$) values of different devices are 0.78 for **1**/N719, 0.74 for **2**/N719 and 0.61 for N719, which was calculated by the following equation:

$$\eta_{cc} = \left[1 + \left(\frac{\tau_d}{\tau_e}\right)\right]^{-1}$$

It is found that the charge collection efficiency was increased after co-sensitization. The higher $\eta_{cc}$ value helps to understand the enhanced IPCE response of the **1**/N719 and **2**/N719 co-sensitized cells. Since the IPCE response of the solar cell can be expressed by the equation:

$$IPCE(\lambda) = LHE(\lambda)\eta_{inj}(\lambda)\eta_{cc}(\lambda) = \left(1-10^{-A}\right)\eta_{inj}(\lambda)\eta_{cc}(\lambda)$$

where LHE is the light harvesting efficiency, $\eta_{inj}$ is the electron injection efficiency, $\eta_{cc}$ is the charge collection efficiency, A is the absorbance of the dye on $TiO_2$ at the maximum wavelength.[43] Among these factors, LHE plays a very important role, and it depends on the absorption property of dyes (Fig. 11a). In addition, as discussed above, the electron injection from the photo-excited states of dye to the conduction band of $TiO_2$ is thermodynamically favorable since the LUMO energy levels of both N719 and complexes lie above the conduction band of $TiO_2$. Meanwhile, the absorption of N719 is compensated by complexes, which leads to an enhanced light harvesting efficiency. Herein, the charge collection efficiency is also confirmed to increase after co-sensitization. The absorbed photon-to-current conversion efficiency (APCE) spectra, calculated as IPCE/LHE, are shown in Fig. 11b.[44] As can be seen, the APCE of the cells varies in the same trend with IPCE in the wavelength range with **1**/N719 > **2**/N719 > N719. In a word, complex **1** or **2**, as a co-sensitizer, not only has overcome the deficiency of N719 absorption in the region of ultraviolet and blue-violet, but also has enhanced the charge collection efficiency, which should be responsible for the enhanced IPCE and $J_{sc}$.

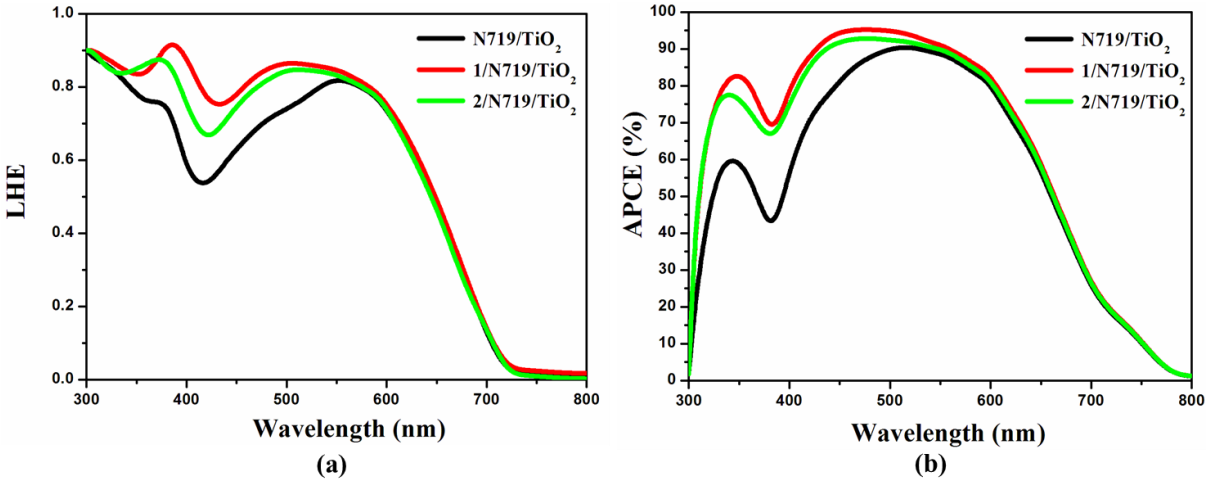


**Fig. 11** (a) The light harvesting efficiency spectra of devices based on single N719 sensitized and co-sensitized photoanodes. (b) The absorbed photon-to-current conversion efficiency spectra of devices based on single N719 sensitized and co-sensitized photoanodes.

Moreover, when the molecular structures of the prepared complexes are taken

into account, it is found that there is a relationship between crystal structure and DSSCs performance. The performance of co-sensitized DSSCs is in the order of **1**/N719 > **2**/N719. This difference in performance is attributed to the changed absorption of prepared complexes caused by different structures. Due to the existence of lone pair electrons, chlorine ion in complex **1** could conjugate with π system to increase the density of electron cloud and lead to the increment of the conjugated delocalized system. Thus, compared to complex **2**, the ultraviolet absorption peak of complex **1** moves toward the long wavelength and the absorption intensity is enhanced. The longer wavelength shift is better for compensating the absorption of N719 and overcoming the competitive light absorption of $I_3^-$, which is better for electronic energy transfer and further enhances the spectra response of N719 on $TiO_2$ films.

## Conclusion

Two new $Cd^{II}$ complexes with multifunctional 4-HIBA ligand have been prepared and investigated as co-sensitizers in a ruthenium dye N719 based solar cell. The cells show photo-electricity conversion efficiencies of 8.27% and 7.73%, which are higher than that for DSSCs using single N719 (6.50%). The improvement in efficiency is attributed to the fact that these complexes can overcome the deficiency of N719 absorption in the region of ultraviolet and blue-violet. Generally, this type of co-sensitization is anticipated to arouse broad interest in further boosting the efficiency of dye-sensitized solar cell by using these important classes of complexes.

## Acknowledgments

This work was supported by National Natural Science Foundation of China (Grant 21371040 and 21171044), the National key Basic Research Program of China (973 Program, No. 2013CB632900), supported by the Fundamental Research Funds for the Central Universities (Grant No. HIT. IBRSEM. A. 201409), and Program for Innovation Research of Science in Harbin Institute of Technology (PIRS of HIT No. A201416 and B201414).

## References

1 X. Y. Huang, S. Y. Han, W. Huang and X. G. Liu, *Chem. Soc. Rev*., 2013, **42**, 173–201.

2 J. Z. Zhang, J. Zhang, H. B. Li, Y. Wu, H. L. Xu, M. Zhang, Y. Geng and Z. M. Su, *J. Power Sources*, 2014, **267**, 300–308.

3 T. Stergiopoulos and P. Falaras, *Adv. Energy Mater*., 2012, **2**, 616–627.

4 L. G. Wei, Y. L. Yang, R. Q. Fan, Y. Na, P. Wang, Y. W. Dong, B. Yang and W. W. Cao, *Dalton Trans.*, 2014, **43**, 11361–11370.

5 Y. Q. Sun, S. Deng, Q. Liu, S. Z. Ge and Y. P. Chen, *Dalton Trans.*, 2013, **42**, 10503–10509.

6 F. A. Almeida Paz, J. Klinowski, S. M. F. Vilela, J. P. C. Tomé, J. A. S. Cavaleiro and J. Rocha, *Chem. Soc. Rev*., 2012, **41**, 1088–1110.

7 C. L. Zhang, L. Qin, Z. Z. Shi and H. G. Zheng, *Dalton Trans.*, 2015, **44**, 4238–4245.

8 J. S. Qin, S. R. Zhang, D. Y. Du, P. Shen, S. J. Bao, Y. Q. Lan and Z. M. Su, *Chem. Eur. J.*, 2014, **20**, 5625–5630.

9 X. F. Zheng, L. Zhou, Y. M. Huang, C. G. Wang, J. G. Duan, L. L. Wen, Z. F. Tian and D. F. Li, *J. Mater. Chem. A*, 2014, **2**, 12413–12422.

10 S. Gao, R. Q. Fan, L. S. Qiang, P. Wang, S. Chen, X. M. Wang and Y. L. Yang, *CrystEngComm*, 2014, **16**, 1113–1125.

11 Y. Feng, D. B. Wang, B. Wan, X. H. Li and Q. Shi, *Inorg. Chim. Acta*, 2014, **413**, 187–193.

12 H. L. Niu, J. T. Chen, Q. Niu, Y. H. Gao, J. M. Song, C. J. Mao, S. Y. Zhang and Q. W. Chen, *J. Cryst. Growth*., 2011, **329**, 82−85.

13 G. X. Liu, X. F. Wang, H. Zhou and S. Nishihara, *Inorg. Chem. Commun.*, 2011, **14**, 1444−1447.

14 J. Z. Zhang, W. R. Cao, J. X. Pan and Q. W. Chen, *Inorg. Chem. Commun.*, 2007, **10**, 1360−1364.

15 J. Fan, Y. A. Zhang, T. Okamura, Z. H. Zou, N. Ueyama and W. Y. Sun, *Inorg. Chem. Commun.*, 2001, **4**, 501−503.

16 D. D. Wang, Y. Wu, H. Dong, Z. X. Qin, D. Zhao, Y. Yu, G. J. Zhou, B. Jiao, Z. X. Wu, M. Gao and G. Wang, *Org. Electron.*, 2013, **14**, 3297–3305.

17 S. P. Singh, K. S. V. Gupta, M. Chandrasekharam, A. Islam, L. Y. Han, S. Yoshikawa, M. Haga, M. S. Roy and G. D. Sharma, *ACS Appl. Mater. Interfaces*, 2013, **5**, 11623–11630.

18 S. Altobello, R. Argazzi, S. Caramori, C. Contado, S. Da Fré, P. Rubino, C. Choné, G. Larramona and C. A. Bignozzi, *J. Am. Chem. Soc.*, 2005, **127**, 15342–15343.

19 T. Banerjee, A. K. Biswas, T. S. Sahu, B. Ganguly, A. Das and H. N. Ghosh, *Dalton Trans.*, 2014, **43**, 13601–13611.
20 S. Archer and J. A. Weinstein, *Coord. Chem. Rev.*, 2012, **256**, 2530–2561.
21 S. Gao, R. Q. Fan, X. M. Wang, L. S. Qiang, L. G. Wei, P. Wang, H. J. Zhang, Y. L. Yang and Y. L. Wang, *J. Mater. Chem. A*, 2015, **3**, 6053–6063.
22 W. X. Yin, Y. T. Liu, Y. J. Ding, Q. Lin, X. M. Lin, C. L. Wu, X. D. Yao and Y. P. Cai, *CrystEngComm*, 2015, **17**, 3619–3626.
23 L .L. Liu, C. X. Yu, F. J. Ma, Y. R. Li, .J. J. Han, L. Lin and L. F. Ma, *Dalton Trans.*, 2015, **44**, 1636–1645.
24 J. Yang, J. F. Ma, Y. Y. Liu and S. R. Batten, *CrystEngComm*, 2009, **11**, 151–159.
25 F. Wang, X. M. Jing, B. Zheng, G. H. Li, G. Zeng, Q. S. Huo and Y. L. Liu, *Cryst. Growth Des.*, 2013, **13**, 3522−3527.
26 X. Du, R. Q. Fan, X. M. Wang, L. S. Qiang, P. Wang, S. Gao, H. J. Zhang, Y. L. Yang and Y. L. Wang, *Cryst. Growth Des.*, 2015, **15**, 2402−2412.
27 D. B. Kuang, S. Ito, B. Wenger, C. Klein, J. E. Moser, R. Humphry-Baker, S. M. Zakeeruddin and M. Grätzel, *J. Am. Chem. Soc.*, 2006, **128**, 4146–4154.
28 X. J. Sang, J. S. Li, L. C. Zhang, Z. J. Wang, W. L. Chen, Z. M. Zhu, Z. M. Su and E. B. Wang, *ACS Appl. Mater. Interfaces*, 2014, **6**, 7876–7884.
29 G. D. Sharma, S. P. Singh, R. Kurchania and R. J. Ball, *RSC Adv.*, 2013, **3**, 6036–6043.
30 C. Y. Lin, C. F. Lo, L. Luo, H. P. Lu, C. S. Hung and E. W. G. Diau, *J. Phys. Chem. C*, 2009, **113**, 755–764.
31 C. M. Cardona, W. Li, A. E. Kaifer, D. Stockdale and G. C. Bazan, *Adv. Mater.*, 2011, **23**, 2367–2371.
32 K. R. Justin Thomas, Y. C. Hsu, J. T. Lin, K. M. Lee, K. C. Ho, C. H. Lai, Y. M. Cheng and P. T. Chou, *Chem. Mater.*, 2008, **20**, 1830–1840.
33 C. M. Cardona, W. Li, A. E. Kaifer, D. Stockdale and G. C. Bazan, *Adv. Mater.*, 2011, **23**, 2367–2371.
34 A. Hagfeldt, G. Boschloo, L. C. Sun, L. Kloo and H. Pettersson, *Chem. Rev.*, 2010, **110**, 6595–6663.
35 J. H. Zhao, X. C. Yang, Y. Hao, M. Cheng, J. Tian and L. C. Sun, *ACS Appl. Mater. Interfaces*, 2014, **6**, 3907–3914.
36 L. Q. Ming, H. Yang, W. J. Zhang, X. W. Zeng, D. H. Xiong, Z. Xu, H. Wang, W. Chen, X. B. Xu, M. K. Wang, J. Duan, Y. B. Cheng, J. Zhang, Q. L. Bao, Z. H.

Wei and S. H. Yang, *J. Mater. Chem. A*, 2014, **2**, 4566–4573.

37 S. A. Haque, E. Palomares, B. M. Cho, A. N. M. Green, N. Hirata, D. R. Klug and J. R. Durrant, *J. Am. Chem. Soc.*, 2005, **127**, 3456–3462.

38 S. E. Koops, B. C. O'Regan, P. R. F. Barnes and J. R. Durrant, *J. Am. Chem. Soc.*, 2009, **131**, 4808–4818.

39 J. Bisquert, A. Zaban, M. Greenshtein and I. Mora-Sero, *J. Am. Chem. Soc*., 2004, **126**, 13550–13559.

40 D. B. Kuang, S. Uchida, R. Humphry-Baker, S. M. Zakeeruddin and M. Grätzel, *Angew. Chem. Int. Ed*., 2008, **47**, 1923–1927.

41 M. Adachi, M. Sakamoto, J. T. Jiu, Y.Ogata and S. Isoda, *J. Phys. Chem. B*, 2006, **110**, 13872–13880.

42 S. P. Singh, K. S. V. Gupta, M. Chandrasekharam, A. Islam, L. Y. Han, S. Yoshikawa, M. Haga, M. S. Roy and G. D. Sharma, *ACS Appl. Mater. Interfaces*, 2013, **5**, 11623–11630.

43 H. Kusama, M. Kurashige, K. Sayama, M. Yanagida and H. Sugihara, *J. Photoch. Photobio. A*, 2007, **189**, 100–104.

44 R. Ghosh, M. K. Brennaman, T. Uher, M. R. Ok, E. T. Samulski, L. E. McNeil, T. J. Meyer and R. Lopez, *ACS Appl. Mater. Interfaces*, 2011, **3**, 3929–3935.